Inorganic Chemistry
Article

Inorg. Chem. **2010**, *49*, 6917–6924 **6917**
DOI: 10.1021/ic1004819

First-Principles Study of the Electronic, Optical Properties and Lattice Dynamics of Tantalum Oxynitride

Pan Li,[†] Weiliu Fan,*[,‡] Yanlu Li,[†] Honggang Sun,[†] Xiufeng Cheng,[†] Xian Zhao,*[,†] and Minhua Jiang[†]

[†]*State Key Laboratory of Crystal Materials, Shandong University, Jinan, 250100, China, and*
[‡]*School of Chemistry and Chemical Engineering, Shandong University, Jinan, 250100, China*

Received March 13, 2010

First-principles calculations of the electronic, optical properties and lattice dynamics of tantalum oxynitride are performed with the density functional theory plane-wave pseudopotential method. The analysis of the electronic structure shows a covalent nature in Ta−N bonds and Ta−O bonds. The hybridization of anion 2p and Ta 5d states results in enhanced dispersion of the valence band, raising the top of the valence band and leading to the visible-light response in TaON. It has a high dielectric constant, and the anisotropy is displayed obviously in the lower energy region. Our calculation indicated that TaON has excellent dielectric properties along [010] direction. Various optical properties, including the reflectivity, absorption coefficient, refractive index, and the energy-loss spectrum are derived from the complex dielectric function. We also present phonon dispersion relation, zone-center optical mode frequency, density of phonon states, and some thermodynamic properties. The experimental IR modes (B_u at 808 cm^{-1} and A_u at 863 cm^{-1}) are reproduced well and assigned to a combination of stretching and bending vibrations for the Ta−N bond and Ta−O bond. The thermodynamic properties of TaON, such as heat capacity and Debye temperature, which were important parameters for the measurement of crystal physical properties, were first given for reference. Our investigations provide useful information for the potential application of this material.

1. Introduction

Modern materials science aims at the development of multifunctional materials designed for application in different industrial branches. This challenging task could be reached by the combination of many desirable properties in one material. Transition metal oxynitrides (TM−O−N) are considered promising multifunctional materials. A variety of the potential applications anticipated for metal oxynitrides (electrochromic coatings, biocompatible coatings, nanocrystalline solar cells and catalysts, and selective solar absorbers[1−4]) is a result of the wide range of chemical compositions of TM−O−N determining their physical, chemical, and functional properties. Recently, it was shown that TM−O−N (TM = Ti, Zr, Hf, Ta) films exhibit improved optical properties compared to pure oxides.[5] In particular, tantalum oxy-nitride (TaON) is a uniquely versatile material with a large number of technological applications, e.g., as decorative coatings,[6] as charge capacitors in dynamic random access memory devices,[7] as gate oxides in microelectronic devices,[8,9] and as visible-light responsive photocatalysts.[10−13] The most prominent characteristic of TaON is the high dielectric constant. The high dielectric constant gate oxide can replace the conventional SiO_2 gate oxide, which would allow the gate oxide to increase its capacitance without having to reduce its thickness.

Tantalum oxynitride has also been the subject of several theoretical investigations. Up to now, most of the works are

*To whom all correspondences should be addressed. Tel.: 86-531-88366330. Fax: 86-531-88364864. E-mail: fwl@sdu.edu.cn (W.F.), zhaoxian@icm.sdu.edu.cn (X.Z.).

(1) Tsyganov, T, I.; Maitz, M. F.; Wieser, E.; Richter, E.; Reuther, H. *Surf. Coat. Technol.* **2005**, *200*, 1041–1044.
(2) Mientus, R.; Grötschel, R.; Ellmer, K. *Surf. Coat. Technol.* **2005**, *200*, 341–345.
(3) Aegerter, M. A. *Sol. Energy Mater. Sol. Cells* **2001**, *68*, 401–422.
(4) Assmann, W.; Reichelt, Th; Eisenhammer, T.; Huber, H.; Mahr, A.; Schellinger, H.; Wolgemuth, R. *Nucl. Instrum. Methods Phys. Res., B* **1996**, *113*, 303–307.
(5) Venkataraj, S.; Severin, D.; Mohamed, S. H.; Ngaruiya, J.; Kappertz, O.; Wuttig, M. *Thin Solid Films* **2006**, *502*, 228–234.
(6) Vaz, F.; Cerqueira, P.; Rebouta, L.; Nascimento, S. M. C.; Alves, E.; Goudeau, Ph.; Rivière, J. P.; Pischow, K.; De Rijk, J. *Thin Solid Films* **2004**, *449*, 447–448.
(7) Cho, S. L.; Kim, B. S.; Kim, H. M.; Chun, I. K.; Kim, K. B. *J. Electrochem. Soc.* **2002**, *149*, C529.
(8) Le Dreo, H.; Banakh, O.; Keppner, H.; Steinmann, P.-A.; Briand, D.; de Rooij, N. F. *Thin Solid Films* **2006**, *515*, 952–956.
(9) Kato, K.; Toyota, H.; Jin, Y.; Ono, T. *Vacuum* **2009**, *83*, 592–595.
(10) Hitoki, G.; Takata, T.; Kondo, J. N.; Hara, M.; Kobayashi, H.; Domen, K. *Chem. Commun.* **2002**, *2002*, 1698–1699.
(11) Hara, M.; Chiba, E.; Ishikawa, A.; Takata, T.; Kondo, J. N.; Domen, K. *J. Phys. Chem. B* **2003**, *107*, 13441–13445.
(12) Hara, M.; Hitoki, G.; Takata, T.; Kondo, J. N.; Kobayashi, H.; Domen, K. *Catal. Today* **2003**, *78*, 555–560.
(13) Chun, W.-J.; Ishikawa, A.; Fujisawa, H.; Takata, T.; Kondo, J. N.; Hara, M.; Kawai, M.; Matsumoto, Y.; Domen, K. *J. Phys. Chem. B* **2003**, *107*, 1798–1803.

Published on Web 06/28/2010

devoted to the electronic structure, high-pressure phases, structure, and stability of its polymorphs.[14−20] However, in contrast to the extensive optical experimental measurements,[8,9,21] there is no corresponding theoretical report concerning the optical properties of crystalline TaON. The optical properties, such as the absorption spectrum and the dielectric function, can be used to determine the optical band gap and electronic dielectric constants, which are fundamental in the modeling of the conduction band offsets, leakage current, and dielectric breakdown.

In addition, the knowledge of lattice dynamic properties plays a key role in understanding the structural, phase transition, infrared (IR)/Raman vibration, optical, and thermodynamic properties. Raman and infrared data have become powerful and effective tools for resolving the structure of the local arrangements by comparison with analogous crystalline compounds. However, theoretical studies of the lattice dynamic and thermodynamic properties of TaON, such as heat capacity and Debye temperature, have rarely been referenced. Systemic studies on lattice dynamics and thermodynamics of TaON are of great importance and in demand.

In this paper, we present a series of first-principles calculations on the electronic, optical, and lattice dynamics properties of tantalum oxynitride. The electronic structures are then calculated from the perspective of the optical properties and are found to depend on both the interband and intraband transitions determined by the energy bands. The optical properties, such as the dielectric function, reflectivity, absorption, refractive index, and electron energy-loss function are discussed. We also discussed the vibrational properties in detail. Finally, some thermodynamic properties such as constant volume heat capacity and Debye temperature are given.

The remainder of this paper is organized as follows. A brief description of our computational method is given in section 2. The results and discussion are examined in section 3, followed by a summary of our conclusions in section 4.

2. Computational Details

The calculations were performed using the plane-wave pseudopotential DFT method as implemented in the CASTEP code,[22] using norm-conserving pseudopotentials[23] and a plane-wave expansion of the wave functions. We used the local-density approximation (LDA) with the Ceperley-Alder[24] form to describe the exchange and correlation potential. The convergence criteria for structure optimization and energy calculation were set to ultrafine quality with a kinetic energy cutoff of 990 eV and k-point meshes of $6 \times 6 \times 6$ for TaON. Geometry optimization was done before single point energy calculation, and the self-consistent convergence accuracy was set at 5.0×10^{-6} eV/atom. The convergence criterion for the maximal force between atoms was 0.01 eV/Å. The maximum displacement was 5.0×10^{-4} Å, and the stress was 0.02 GPa. For the equilibrium structure, the Mulliken populations were investigated using a projection of the plane-wave states onto a linear combination of atomic orbital basis sets,[25,26] which is widely used to perform charge transfers and population analyses. The electronic band structures, densities of state (DOS) spectra, and optical properties are also derived under the optimized structures. The phonon frequencies and densities of phonon state were calculated from the response to small atomic displacements.[27]

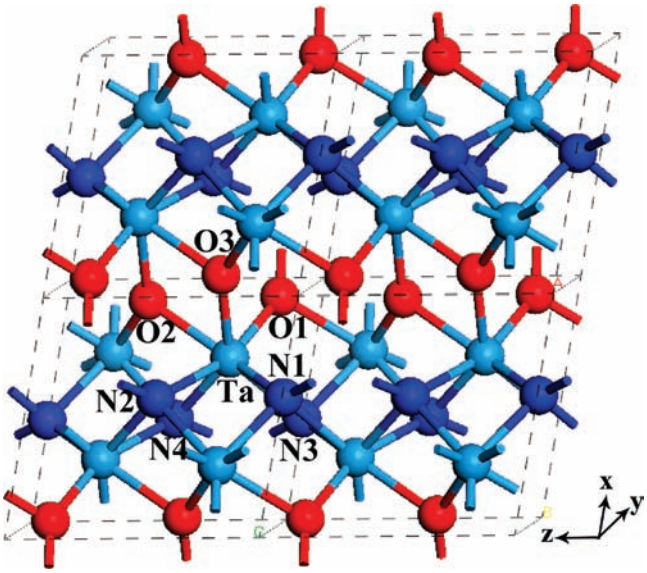

Figure 1. Crystal structure of TaON (light blue, red, and dark blue colors represent Ta, O, and N atoms, respectively).

3. Results and Discussion

3.1. Structural and Electronic Properties. TaON is known to crystallize in the monoclinic baddeleyite structure with space group $P2_1/c$. Powder neutron diffraction experiments revealed that the oxygen and nitrogen atoms of TaON have an ordered arrangement.[28] As shown in Figure 1, the tantalum atom experiences 7-fold coordination by three oxygen atoms and four nitrogen atoms. By minimizing the crystal total energy, the equilibrium lattice parameter has been computed, and the results are given in Table 1 with the experimental values. The equilibrium structural parameters are in very good agreement with experimental values within deviations of 3.0% in the lattice constants.

As for the complicated chemical bonding behavior in TaON, we performed the corresponding Mulliken charge and bond population to analyze the bonding character

(14) Fang, C. M.; Orhan, E.; de Wijs, G. A.; Hintzen, H. T.; de Groot, R. A.; Marchand, R.; Saillard, J.-Y.; de With, G. *J. Mater. Chem.* **2001**, *11*, 1248–1252.
(15) Lumey, M.-W.; Dronskowski, R. *Z. Anorg. Allg. Chem.* **2003**, *629*, 2173–2179.
(16) Lumey, M.-W.; Dronskowski, R. *Z. Anorg. Allg. Chem.* **2005**, *631*, 887–893.
(17) Schilling, H.; Stork, A.; Irran, E.; Wolff, H.; Bredow, T.; Dronskowski, R.; Lerch, M. *Angew. Chem., Int. Ed.* **2007**, *46*, 2931–2934.
(18) Wolff, H.; Bredow, T.; Lerch, M.; Schilling, H.; Irran, E.; Stork, A.; Dronskowski, R. *J. Phys. Chem. A* **2007**, *111*, 2745–2749.
(19) Bredow, T.; Lumey, M.-W.; Dronskowski, R.; Schilling, H.; Pickardt, J.; Lerch, M. *Z. Anorg. Allg. Chem.* **2006**, *632*, 1157–1162.
(20) Lowther, J. E. *Phys. Rev. B* **2006**, *73*, 134110.
(21) Banakh, O.; Steinmann, P.-A.; Dumitrescu-Buforn, L. *Thin Solid Films* **2006**, *513*, 136–141.
(22) Segall, M. D.; Lindan, P. L. D.; Probert, M. J.; Pickard, C. J.; Hasnip, P. J.; Clark, S. J.; Payne, M. C. *J. Phys. B: Condens. Matter* **2002**, *14*, 2717–2744.
(23) Vanderbilt, D. *Phys. Rev. B* **1990**, *41*, 7892–7895.
(24) Ceperley, D. M.; Alder, B. J. *Phys. Rev. Lett.* **1980**, *45*, 566–569.
(25) Sanchez-Portal, D.; Artacho, E.; Soler, J. M. *Solid State Commun.* **1995**, *95*, 685–690.
(26) Segall, M. D.; Shah, R.; Pickard, C. J.; Payne, M. C. *Phys. Rev. B* **1996**, *54*, 16317–16320.
(27) Gonze, X. *Phys. Rev. B.* **1997**, *55*, 10337–10354.
(28) Armytage, D.; Fender, B. E. F. *Acta Crystallogr., Sect. B* **1974**, *30*, 809.

Table 1. Structure Parameters of TaON: Lattice Parameters and Atom Positions

		present				experiment[28]		
lattice parameters	*a* (Å)	*b* (Å)	*c* (Å)	*β* (deg)	*a* (Å)	*b* (Å)	*c* (Å)	*β* (deg)
	4.8194	4.9007	5.0580	99.97	4.9581	5.0267	5.1752	99.64
		x	*y*	*z*		*x*	*y*	*z*
atom positions	Ta (4e)	0.2915	0.0508	0.2181	Ta (4e)	0.2920	0.0460	0.2130
	O (4e)	0.0612	0.3251	0.3493	O (4e)	0.0640	0.3240	0.3450
	N (4e)	0.4419	0.7555	0.4766	N (4e)	0.4449	0.7566	0.4810

Table 2. Mulliken Charge (|*e*|) and Bond Population of TaON

species	s	p	d	total	charge	bonds	population	length (Å)
Ta	0.39	0.20	3.10	3.70	1.30	O1−Ta	0.59	2.033
						O2−Ta	0.34	2.165
O	1.83	4.77	0.00	6.60	−0.60	O3−Ta	0.40	2.092
						N1− Ta	0.54	2.072
N	1.69	4.01	0.00	5.70	−0.70	N2− Ta	0.43	2.177
						N3− Ta	0.50	2.129
						N4− Ta	0.41	2.105

quantitatively. It is well-known that the absolute magnitudes of the atomic charges yielded by the population analysis have little physical meaning, since they are highly sensitive to the atomic basis set. But we still can find some useful information by considering the relative values of Mulliken population. The results are given in Table 2. The Mulliken charges transferred from Ta atoms to N atoms and O atoms are 0.70 and 0.60*e*, respectively. From the charge transfer, we can infer that the N atoms are more electron affinitive than O atoms. The overlap population between the N−Ta atoms is 0.54*e*, 0.43*e*, 0.50*e*, and 0.41*e*, and the bonding shows the covalent nature. The O−Ta bonding also shows the covalent nature whose overlap population is 0.59*e*, 0.34*e*, and 0.40*e*. It is indicated that the covalency between Ta and N is greater than between Ta and O. This kind of difference could affect the band gap positions of TaON.

The calculated band structure and density of states (DOS) spectra of TaON are shown in Figures 2 and 3, respectively. From Figure 2, we can see that it is an indirect band gap semiconductor with an indirect band gap of 1.92 eV along the G direction to the B point. The direct band gap at the highly symmetric G point is 2.25 eV, which is slightly smaller than 2.4 eV from the measurements of diffuse reflectance spectra.[29] The band gap underestimation of DFT always exists due to the well-known limitation of predicting accurate conduction band properties.[30] Figure 3 shows the total and partial density of states of TaON. The lowest-lying states (−19.3 to −17.3 eV) stem from the O 2s states with less contributions from the Ta dsp-hybridized states, and the states in the higher energy range (−15.2 to −12.6 eV) are essentially contributed by the N 2s states with contributions from the Ta dsp-hybridized states. The PDOSs in the region of −7.7 to 0 eV mainly come from the O 2p and N 2p orbitals with contributions from Ta 5d orbitals, indicating the potential covalent bonding character in the compound. We can see that the top of the valence band is dominated by N 2p states.

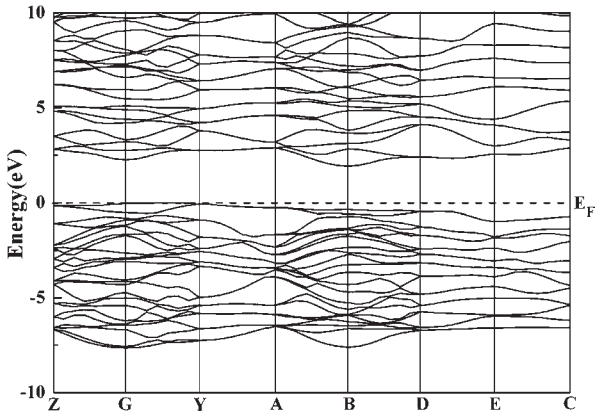

Figure 2. Electronic band structures of TaON.

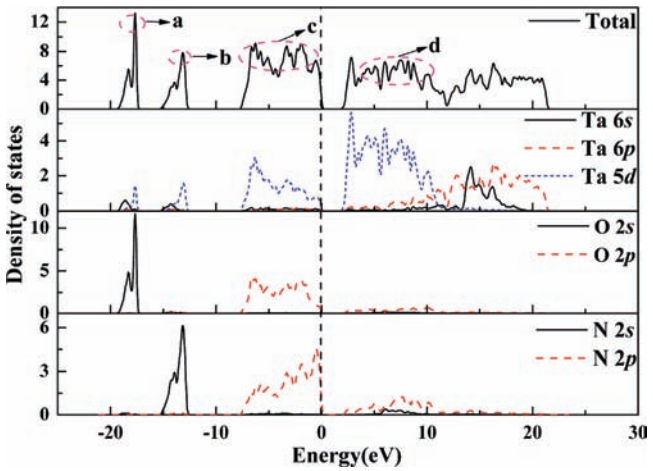

Figure 3. Total and partial densities of states of TaON.

That is in agreement with the Mulliken analysis results; that is, the stronger covalency between Ta and N could affect the band gap positions of TaON. It is noted that there is a large dispersion of the valence band by the hybridization of O 2p and N 2p orbitals with Ta 5d orbitals. The large dispersion of the valence band raises the top of the valence band, which is responsible for the visible-light response in TaON. The bottom of the conduction band is mainly composed of Ta 5d orbitals hybridized with O 2p and N 2p orbitals. Due to the different energies of Ta 5d, O 2p, and N 2p orbitals, the PDOS for Ta 5d, O 2p and N 2p orbitals shows their asymmetric distribution in the bonding and antibonding bands. The bonding band has a larger O 2p and N 2p contribution, and vice versa, the antibonding band has a larger Ta 5d contribution.

(29) Orhan, E.; Tessier, F.; Marchand, R. *Solid State Sci.* **2002**, *4*, 1071–1076.
(30) Martin, R. M. *Electronic Structure: Basic Theory and Practical Methods*; Cambridge University Press: Cambridge, England, 2004.

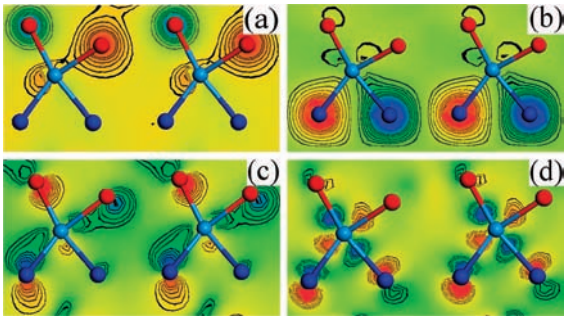

Figure 4. Charge density contour maps for various electronic states of TaON (light blue, red, and dark blue colors represent Ta, O, and N atoms, respectively) corresponding to the selected energy range (a, b, c, d) marked with ellipses in the DOS. The contour levels are uniformly spaced starting at -0.12 e/Å^3, with a spacing of 0.002 e/Å^3 between contours.

For getting a further understanding about the bonding character of the system, we have constructed the charge density contour maps associated with the selected states (a, b, c, d) marked with ellipses in the DOS of Figure 3, as it is shown in Figure 4. We chose to construct contour plots in the plane containing Ta, O1, O2, N1, and N2 atoms. From these plots, we can see the character of σ bonding states in the valence band and the corresponding σ^* antibonding states in the conduction band. Figure 4a showed that there is an obvious directional bonding between the Ta atoms and O atoms. Combined with the DOS analysis, it can be concluded that the σ bonding states formed from the O 2s states and Ta dsp-hybridized states in the region of -19.3 to -17.3 eV. There is also a directional bonding between the Ta atoms and N atoms in Figure 4b, which showed that the σ bonding states formed from the N 2s states and Ta dsp-hybridized states in the region of -15.2 to -12.6 eV. In the energy states -7.7 to 0 eV close to the top of the valence band, the σ bonding states came from the anion 2p states with somewhat less density associated with the Ta dsp-hybridized states, as shown in Figure 4c. We can see the corresponding σ^* antibonding states in the region of 3.5−10.2 eV in Figure 4d, which are formed from the Ta dsp-hybridized states with a small contribution from the anion 2p states in the conduction band. That corresponds with the DOS analysis results, showing the asymmetric distribution in the bonding and antibonding bands. From the above information, we can infer that the formation of a 7-fold coordination polyhedron around Ta stems from the bonding between the Ta dsp-hybridized states and three N 2p states, two O 2p states, one N 2s state, and one O 2s state.

3.2. Optical Properties. The optical properties of TaON are determined by the dielectric function $\varepsilon(\omega) = \varepsilon_1(\omega) + i\varepsilon_2(\omega)$ that is mainly contributed from the electronic structures. The imaginary part, $\varepsilon_2(\omega)$, of the dielectric function $\varepsilon(\omega)$ is calculated from the momentum matrix elements of transition between the occupied and unoccupied electronic states and is given by

$$\varepsilon_2 = \frac{2e^2\pi}{\Omega\varepsilon_0}\sum_{k,v,c}|\langle\psi_k^c|\hat{u}r|\psi_k^v\rangle|^2\delta(E_k^c - E_k^v - E) \quad (1)$$

where Ω is the unit cell volume, $\hat{u}$ is the vector defining the polarization of the incident electric field, ω is the light frequency, e is the electronic charge, and ψ_k^c and ψ_k^v are the conduction and valence band wave functions at k, respectively. Since the dielectric function describes the causal response, the real and imaginary parts are linked using the Kramers−Kronig transform. The real part $\varepsilon_1(\omega)$ of the dielectric function can be derived from the imaginary part $\varepsilon_2(\omega)$ with the causal transform. All of the other optical properties, such as the reflectivity $R(\omega)$, the absorption spectrum $\alpha(\omega)$, the real part of the refractive index $n(\omega)$, the imaginary part of the refractive index $k(\omega)$, and the electron energy-loss spectrum $L(\omega)$ can be derived from $\varepsilon_1(\omega)$ and $\varepsilon_2(\omega)$

$$R(\omega) = \left|\frac{\sqrt{\varepsilon_1(\omega)+j\varepsilon_2(\omega)}-1}{\sqrt{\varepsilon_1(\omega)+j\varepsilon_2(\omega)}+1}\right|^2 \quad (2)$$

$$\alpha(\omega) = \sqrt{2}\omega\left[\sqrt{\varepsilon_1^2(\omega)+\varepsilon_2^2(\omega)}-\varepsilon_1(\omega)\right]^{\frac{1}{2}} \quad (3)$$

$$n(\omega) = \left[\sqrt{\varepsilon_1^2(\omega)+\varepsilon_2^2(\omega)}+\varepsilon_1(\omega)\right]^{\frac{1}{2}}/\sqrt{2} \quad (4)$$

$$k(\omega) = \left[\sqrt{\varepsilon_1^2(\omega)+\varepsilon_2^2(\omega)}-\varepsilon_1(\omega)\right]^{\frac{1}{2}}/\sqrt{2} \quad (5)$$

$$L(\omega) = \varepsilon_2(\omega)/[\varepsilon_1^2(\omega)+\varepsilon_2^2(\omega)] \quad (6)$$

In the high dielectric constant materials, the large static constant is mostly of vibrational origin. The value $\varepsilon(0) = \varepsilon_{\omega\to\infty} + \varepsilon_{\omega=0}$ is dominated by the lattice vibrational component $\varepsilon_{\omega=0}$ (typically upward of 10−15) over the electronic contribution $\varepsilon_{\omega\to\infty}$ (typically 3−5). The lattice part depends quadratically on the ratio of effective dynamical charges (polarization change upon atomic motion) to the frequency of infrared active modes[31,32]

$$\varepsilon_{\omega=0}^{\alpha\beta} = \frac{4\pi e^2}{\Omega}\sum_{\lambda}\frac{z_{\lambda\alpha}z_{\lambda\beta}}{\omega_\lambda^2} \quad (7)$$

with the mode charge vector

$$z_{\lambda\beta} = \sum_{i\beta}\frac{Z^*_{i,\alpha\beta}\xi_{i,\lambda\beta}}{\sqrt{M_i}}$$

the system volume Ω, the effective charge tensor $\vec{Z}_i^*$, the mass of the i atom M_i, the eigenvector $\vec{\xi}$ and eigenfrequency ω of mode λ, and Cartesian indexes α and β.

The real part of the dielectric function $\varepsilon_1(\omega)$ and the imaginary part $\varepsilon_2(\omega)$ are plotted in Figure 5; from the real part $\varepsilon_1(\omega)$ of the dielectric function, we can obtain the electronic contribution of the dielectric constants, which is about 9.0 in our calculation, combining with the lattice vibration contribution of 21.6 calculated from linear responses method within the density functional perturbation theory (DFPT). The total static dielectric constant is 30.6, which indicates that TaON is a high dielectric constant

(31) See, e.g.: Zhao, X.; Vanderbilt, D. *Phys. Rev. B* **2002**, *65*, 075105. Zhao, X.; Vanderbilt, D. *Phys. Rev. B* **2002**, *65*, 233106.
(32) Bruesch, P. *Phonon: Theory and Experiments-II*; Springer: Berlin, 1986.

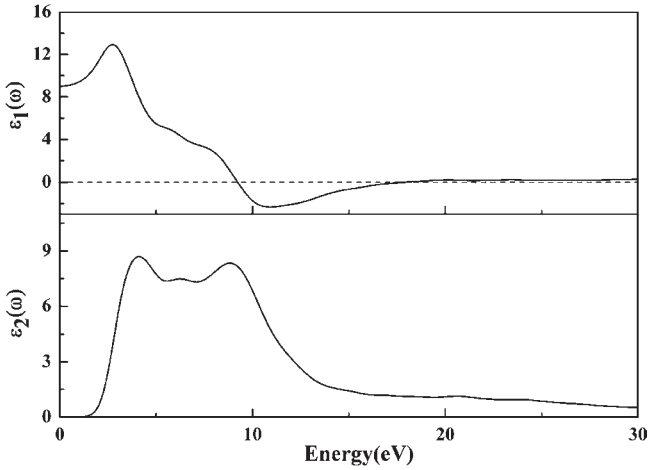

Figure 5. Real $\varepsilon_1(\omega)$ and imaginary $\varepsilon_2(\omega)$ parts of the dielectric function $\varepsilon(\omega)$ of TaON.

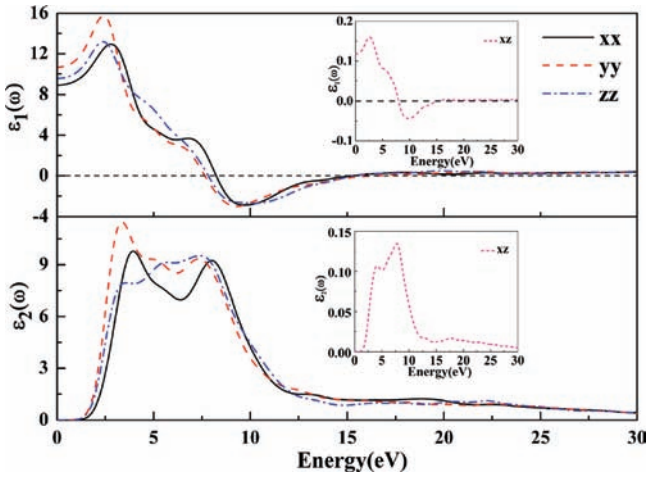

Figure 6. Real $\varepsilon_1(\omega)$ and imaginary $\varepsilon_2(\omega)$ parts of the dielectric function $\varepsilon(\omega)$ of TaON corresponding to different directions: ε^{xx} (black line), ε^{yy} (red line), and ε^{zz} (blue line). The inset shows off-diagonal element ε^{xz} (magenta line).

material, corresponding well with an experimental value over 30.[9] The $\varepsilon_1(\omega)$ of TaON indicates an obvious peak below zero at 10.9 eV, at which the material exhibits metallic properties. In the imaginary part $\varepsilon_2(\omega)$, there are two main peaks at around 4.1 and 8.8 eV, mainly from the electron transitions between the Ta 5d and 2p orbitals of the anion.

Due to the anisotropy of the monoclinic crystal, the dielectric function $\varepsilon(\omega)$ of TaON has four nontrivial components: ε^{xx}, ε^{yy}, ε^{zz}, and ε^{xz}, as it is shown in Figure 6. The off-diagonal component ε^{xz} is much smaller than the diagonal components. The anisotropy in the diagonal components ε^{xx}, ε^{yy}, and ε^{zz} occurs mainly in the energy region 0−10 eV, and in the higher energy region, the anisotropy is not displayed obviously. There are two peaks at 4.4 and 9.3 eV for $\varepsilon_2{}^{xx}$, whereas $\varepsilon_2{}^{yy}$ peaks at 3.7 and 8.6 eV. Table 3 shows the optical-frequency ($\omega\rightarrow\infty$) and low-frequency ($\omega = 0$) dielectric tensors of TaON. The static dielectric tensor $\varepsilon(0)$ is calculated by adding the lattice vibration contribution to the electronic dielectric tensor. The component of $\varepsilon^{yy}(0)$ is 38.97, which is much bigger than the other components. It is indicated that TaON has

Table 3. Optical-Frequency ($\omega \rightarrow \infty$) and Low-Frequency ($\omega = 0$) Dielectric Tensors of TaON

$\omega \rightarrow \infty$			$\omega = 0$		
x	*y*	*z*	*x*	*y*	*z*
8.43	0	0.11	19.70	0	1.62
0	9.85	0	0	29.12	0
0.11	0	8.80	1.62	0	18.91

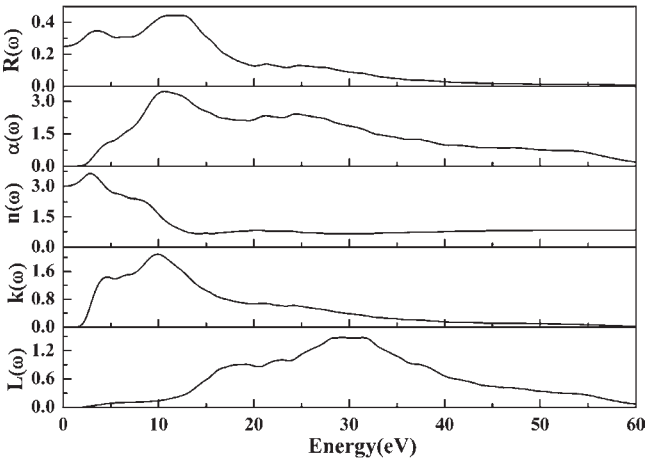

Figure 7. Reflectivity $R(\omega)$, absorption spectrum $\alpha(\omega)$, real part of the refractive index $n(\omega)$, imaginary part of the refractive index $k(\omega)$, and electron energy-loss spectrum $L(\omega)$ of TaON.

excellent dielectric properties along the [010] direction, which may provide an optical metrology for gate dielectric films on silicon substrates.

Figure 7 shows the reflectivity $R(\omega)$, absorption spectrum $\alpha(\omega)$, real part of the refractive index $n(\omega)$, imaginary part of the refractive index $k(\omega)$, and electron energy-loss spectrum $L(\omega)$ of TaON. The reflectivity spectrum shows two main peaks at 3.6 and 11.3 eV, which could be interpreted as the interband transitions and the electron transitions from the valence to conduction bands, respectively. The absorption coefficient indicates the fraction of energy lost by the electromagnetic wave when it passes through a unit thickness of the material, and it is proportional to the rate of Joule heat produced in the sample. In our calculation, we only consider the eigen absorption, without considering the polarized absorption, which has a minor influence on the spectrum. The steepest increase in the absorption coefficient defines the optical band gap, and a value of 2.3 eV is extracted from our calculation. The absorption band of TaON is from 2.2 to 60 eV. Above 2.2 eV, the absorption increases continuously before reaching a maximum. In the high-energy region (above 60 eV), the crystal is transparent because it progressively becomes more difficult for the electrons to respond. The refractive index is displayed, and the static refractive index $n(0)$ is found to have a value of 3.0, which is similar to the experimental results over 2.5 at 632.8 nm wavelength for TaON films.[9] TaON has a large refractive index and can be used as a cladding layer. The electron energy-loss function $L(\omega)$ is an important optical parameter describing the energy loss of a fast electron traversing in a certain material. The peaks in the $L(\omega)$ spectra represent the characteristics associated with the plasma resonance, and the corresponding frequency is the so-called plasma frequency,

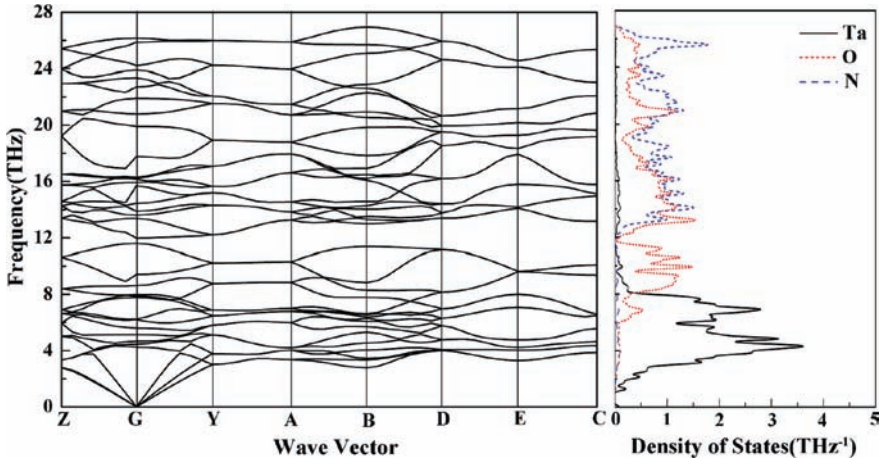

Figure 8. Dispersion curves of phonon and partial phonon density of states for TaON.

above which the material is a dielectric [$\varepsilon_1(\omega) > 0$] and below which the material behaves like a metallic compound in some sense [$\varepsilon_1(\omega) < 0$]. In addition, the peaks of $L(\omega)$ point out the trailing edges in the reflection spectra; for instance, the peak at 19.1 eV corresponds to the abrupt reduction of $R(\omega)$. Unfortunately, the related spectroscopic data, such as parallel electron energy loss spectroscopy, are insufficient at present.

3.3. Lattice Dynamics. Dynamical properties were obtained by the use of linear response method, within density functional perturbation theory (DFPT).[27,33] DFPT is not only one of the most robust methods for the calculation of dynamic properties but also a method that naturally enables the calculation of the second-order derivatives of the total energy with respect to atomic position, and thus the properties of phonon modes to be evaluated directly. The long-range behavior of the Coulomb interaction gives rise to macroscopic electric fields for longitudinal (LO) and transverse (TO) optical phonons, and the coupling between the phonon modes and the electric field leads to the LO−TO splitting at the G point.[34,35] The Born effective tensor is a very important quantity, which determines the well-known phenomenon of LO−TO splitting.[36] LO−TO splitting affects only infrared active modes near the gamma point, raising the frequencies of LO modes above those of TO modes.

Figure 8 shows dispersion curves and partial densities of states of the phonon for TaON. The macroscopic electric field splits the infrared active modes A_u and B_u to transverse A_u (TO) and B_u (TO) and longitudinal A_u (LO) and B_u (LO) components for TaON. Meanwhile, the calculated phonon dispersion relations have no soft mode at any wave vectors, which indicates the stability of the phase. From the partial density of states of the phonon, we can see that the contribution of Ta movements dominates at lower frequencies, while that of O and N movements lies at higher frequencies, since Ta is heavier than O and N.

Table 4. Phonon Frequencies of TaON at G Point

	phonon frequency	
symmetry	present	reference[37]
	Raman	
A_g	142	
B_g	149	
A_g	156	
B_g	187	
A_g	207	
A_g	260	
B_g	266	
B_g	387	
A_g	446	
A_g	454	
B_g	531	
A_g	540	
B_g	544	
A_g	694	
B_g	731	
B_g	779	
A_g	797	
B_g	872	
	IR	
A_u	172	
A_u	208	
B_u(TO)	262	
B_u(LO)	288	
A_u	314	
B_u	399	
B_u	463	
A_u(TO)	482	
B_u	523	
A_u(LO)	539	
B_u	593	
A_u	664	
A_u	758	
B_u	808	782
A_u	863	827

For TaON, the exact phonon frequencies occur at the high symmetry points Z, G, Y, A, B, D, E, and C. Lattice vibration at the G point can be closely investigated by infrared (IR) and Raman spectra. The group symmetry decomposition into irreducible representations of the $P2_1/c$ point group at the G point yields a sum of $A_u + 2B_u$ for three acoustic modes and $9A_g + 9B_g + 8A_u + 7B_u$ for the 33 optical modes, which contain 18 Raman active modes ($9A_g + 9B_g$) and 15 IR-active modes ($8A_u + 7B_u$). Table 4

(33) Baroni, S.; de Gironcoli, S.; Dal Corso, A.; Giannozzi, P. *Rev. Mod. Phys.* **2001**, *73*, 515–562.
(34) Payne, M. C.; Teter, M. P.; Allan, D. C.; Arias, T. A.; Joannopoulos, J. D. *Rev. Mod. Phys.* **1992**, *64*, 1045–1097.
(35) Segall, M.; Lindan, P.; Probert, M.; Pickard, C.; Hasnip, P.; Clark, S.; Payne, M. *J. Phys.: Condens. Matter* **2002**, *14*, 2717–2744.
(36) Parlinski, K.; Li, Z. Q.; Kawazoe, Y. *Phys. Rev. Lett.* **1998**, *81*, 3298.

shows the calculated frequencies at the G point in comparison with previous IR experimental data.[37] In order to have a clear picture of the vibrational patterns; we have illustrated the atom displacements for the modes at various frequencies, as shown in the Supporting Information and Figure 9. The low-frequency region (<200 cm^{-1}) contains one IR mode at 172 cm^{-1}, and from the analysis of vibrational patterns, we find that the Ta atoms along the diagonal axes move in parallel in the same direction, while they move against each other at 142, 149, 156, and 187 cm^{-1} in the Raman modes. There are four modes in the 200−300 cm^{-1} region, the vibration motion is a mixing of bending and stretching. The lower the energy of the vibration, the less pronounced are the stretching modes. The vibration contributions mainly come from the Ta and O atoms, which are consistent with the contribution in the phonon density of states. The A_u mode at 314 cm^{-1} and B_g mode at 387 cm^{-1} arise from the O atoms' movement, while the Ta and N atoms are nearly kept still. In the high-frequency region (395−900 cm^{-1}), stretching modes also occur together with bending modes. The O and N atoms move, whereas the Ta atoms hold almost static. Figure 9 shows the atom displacements for the vibrational modes of B_u at 808 cm^{-1} and A_u at 863 cm^{-1} of TaON, which are verified in the IR experiment.[37] Our calculations agree well with the experimental data, while there seems to be a little shift to the high energy region. As is well-known, the LDA usually underestimates the volume. Therefore, we can conclude that our calculated IR-active modes have a higher frequency than experimental ones by the underestimation of volume with the LDA. The coordination polyhedra around Ta are distorted by the N2 and N4 atoms moving in parallel in the same direction, as well as the N1 and N3 atoms and O2 and O3 atoms. The A_g and B_g modes have inversion symmetry and are thus Raman-active. In these modes, the coordination polyhedra around Ta are distorted by the relative motion of the N2 and N4 atoms, N1 and N3 atoms, and O2 and O3 atoms.

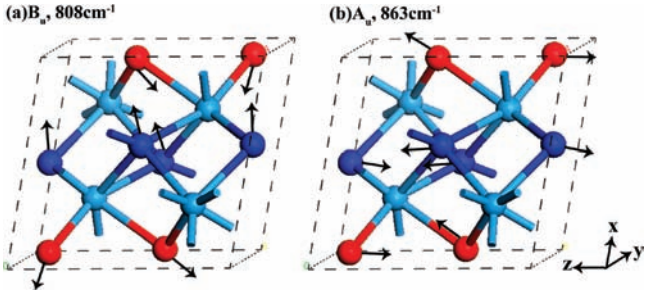

Figure 9. Atom displacements for the vibrational modes of B_u at 808 cm^{-1} (a) and A_u at 863 cm^{-1} (b) of TaON (light blue, red, and dark blue colors represent Ta, O, and N atoms, respectively).

3.4. Thermodynamic Properties. Employing quasiharmonic approximation,[38] we evaluate thermodynamical properties under finite temperatures. The vibrational density of states can be written as

$$g(w) = \frac{\Omega}{(2\pi)^3}\int \frac{dS}{|\nabla_q \omega(q)|} = \frac{\Omega}{(2\pi)^3}\sum_q \frac{\delta}{(\omega-\omega_q)^2+\delta^2} \quad (8)$$

where δ is the adjustable width factor of Lorentzian function. Heat capacity at a constant volume C_v can be calculated directly from the phonon DOS under the harmonic approximation and then can be given by the formula[39]

$$C_v(T) = \int_0^{\omega_{max}} k_B(\frac{\hbar\omega}{k_B T})^2 \frac{\exp(\hbar\omega/k_B T)}{[\exp(\hbar\omega/k_B T)-1]^2} g(\omega)\, d(\omega) \quad (9)$$

Heat capacity at constant volume under the Debye approximation is expressed as follows:[40]

$$C_v = 9N_A k_B (T/\Theta_D)^3 \int_0^{\Theta_D/T} d\nu\, (h\nu/k_B T)^2 W(h\nu/k_B T) \quad (10)$$

where the weighting factor $W(h\nu/k_BT) = (h\nu/k_BT)^2 \exp(h\nu/k_BT)/[\exp(h\nu/k_BT) - 1]^2$ and the Debye temperature at a given temperature was determined by fitting the theoretical C_v to that from this formula.

In Figure 10, we present results on the heat capacity at Constant volume (C_v) and the temperature dependence of the Debye temperature Θ_D for TaON. From plot a, we can see that the heat capacity increases rapidly below 400 K and reaches a maximum of 68.5 J/(mol K) at about 900 K. By fitting the theoretical C_v with the Debye model, we derive the temperature-dependent Debye temperature $\Theta_D(T)$, as it is shown in plot b. The Debye temperature

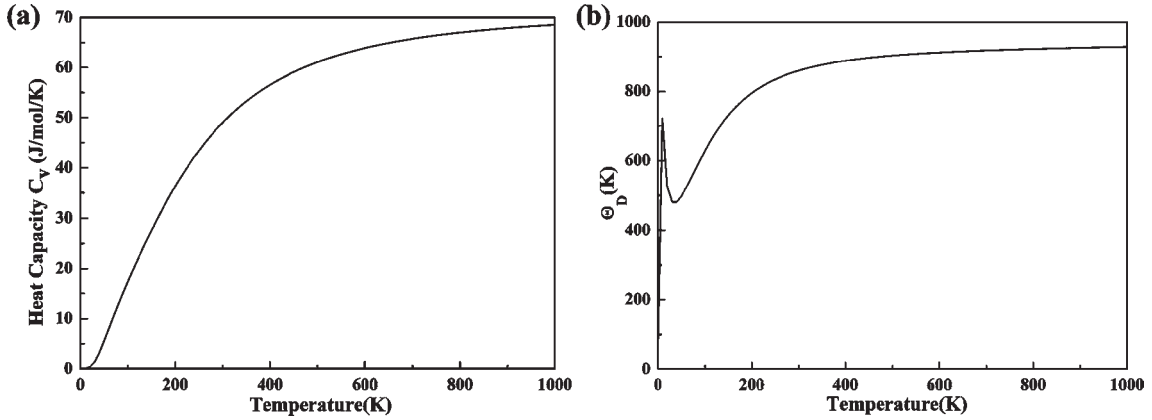

Figure 10. Constant volume heat capacity C_v (a) and temperature dependence of Debye temperature Θ_D (b) for TaON.

is about 920 K, which is an important parameter for the measurement of crystal physical properties.

4. Conclusions

In the present study, first-principles calculations are used to investigate the structure, electronic properties, optical properties, lattice dynamics, and some thermodynamic properties of tantalum oxynitride. The Mulliken charge and bond population further demonstrate covalent bonds between Ta and O atoms and between Ta and N atoms. The hybridization of anion 2p and Ta 5d states attributed to the covalent nature in Ta−N bonds and Ta−O bonds results in enhanced dispersion of the valence band, raising the top of the valence band and leading to the visible-light response in TaON. The analysis of the charge density contour maps shows that the formation of a 7-fold coordination polyhedron around Ta stem from the bonding between the Ta dsp-hybridized states and three N 2p states, two O 2p states, one N 2s state, and one O 2s state. TaON has a high dielectric constant and a high refractive index, and the anisotropy in the optical properties is displayed obviously in the lower energy region. Our calculation indicated that TaON has excellent dielectric properties along the [010] direction. The absorption spectrum exhibits an optical band gap of 2.3 eV. Moreover, it has a large refractive index. The calculated Raman and infrared data provided powerful and effective tools for resolving the structure from analogous crystalline compounds. The experimental IR peaks (B_u at 808 cm^{-1} and A_u at 863 cm^{-1}) are well reproduced and assigned to the movements of N atoms and O atoms with Ta atoms moving slightly. The coordination polyhedra around Ta are distorted by the N2 and N4 atoms moving in parallel in the same direction, as well as the N1 and N3 atoms, and O2 and O3 atoms. The thermodynamic properties of TaON, such as heat capacity and Debye temperature, which were important parameters for the measurement of crystal physical properties, were first given for reference. Our investigations provide useful information for the potential application of this material.

Acknowledgment. This work is supported by the National Natural Science Foundation of China (Grant Nos. 50802056 and 50721002), 973 Program of China under Grant No. 2009CB930103, Youth Scientist (Doctoral) Foundation of Shandong Province of China under Grant No. BS2009CL038, and the Independent Innovation Foundation of Shandong University (IIFSDU) under Grant No. 2009TS016.

Supporting Information Available: Figures giving atom displacements for the vibrational modes. This material is available free of charge via the Internet at http://pubs.acs.org.

(37) Nakamura, R.; Tanaka, T.; Nakato, Y. *J. Phys. Chem. B* **2005**, *109*, 8920–8927.
(38) Maradudin, A. A.; Montroll, E. W.; Weiss, G. H.; Ipatova, I. P. *Theory of Lattice Dynamics in the Harmonic Approximation*, 2nd ed.; Academic: New York, 1971.
(39) Xiao, Y.; Yan, X. H.; Xiang, J.; Mao, Y. L.; Zhang, Y.; Cao, J. X.; Ding, J. W. *Appl. Phys. Lett*. **2004**, *84*, 4626–4628.
(40) Tohei, T.; Kuwabara, A.; Oba, F.; Tanaka, I. *Phys. Rev. B* **2006**, *73*, 064304.